Mixing Quantum-Classical Molecular Dynamics Methods Applied to Intramolecular Proton Transfer in Acetylacetone

OMAR A. SHARAFEDDIN,[1] KONRAD HINSEN,[1,2] TUCKER CARRINGTON, JR.,[1] BENOÎT ROUX[1,2]

[1]*Département de chimie, Université de Montréal, C.P. 6128, succ. Centre-ville H3C 3J7, Canada*
[2]*Groupe de Recherche en Transport Membranaire (GRTM), Département de physique, Université de Montréal, C.P. 6128, succ. Centre-ville H3C 3J7, Canada*

Received 23 January 1997; accepted 29 April 1997

ABSTRACT: We present results of mixed quantum-classical molecular dynamics simulations of the intramolecular proton transfer in acetylacetone. Simulations are performed starting from the reactant and transition state configurations with initial velocities at each configuration chosen from an ensemble at 300 K. The proton motion is treated quantum mechanically and the remaining degrees of freedom are treated classically. Two mixed quantum-classical molecular dynamics methods are implemented. In the first, a quantum-classical time-dependent self-consistent field method (QC/TDSCF), the time-dependent Schrödinger equation for the proton is solved using the split operator approach and a plane-wave basis. In the second, a mixed quantum-classical adiabatic method (QC/A), the instantaneous ground state wave function is calculated by solving the time-independent Schrödinger equation for the configurations of the classical particles by propagating in imaginary time using the split operator approach and the same plane-wave basis. A comparison of the two approaches with classical trajectories is presented. The QC/TDSCF and QC/A results are very similar for trajectories started from the reactant configuration. The two methods, however, yield somewhat different results when the trajectories are started from the transition state configuration. The proton wave function of the QC/A method adjusts instantaneously to the position of the classical particles, whereas the motion of the QC/TDSCF wavepacket more faithfully represents the true proton dynamics. *J Comput Chem* **18**: 1760–1772, 1997

Correspondence to: B. Roux
Contract/grant sponsor: FCAR (Québec)
Contract/grant sponsor: NSERC (Canada)

CCC 0192-8651 / 97 / 141760-13

Keywords: computer simulations; wavepacket; zero-point vibration; activation energy; reaction coordinate; empirical valence bond; Fourier transform

Introduction

Due to their practical importance and special properties proton transfer reactions have been studied intensively.[1–3] Symmetric intramolecular proton transfer reactions of the type (A–H—A) ↔ (A—H–A) are of particular interest. It is much simpler to consider a proton transfer process that occurs in a single molecule because one does not have to deal with the complications associated with the diffusion of multiple donors and acceptors in the liquid phase. From a theoretical point of view, proton transfer processes are especially interesting and challenging because quantum effects, such as zero point motion and tunneling, are expected to be important due to the light mass of the hydrogen nucleus. As quantum-mechanical calculations are difficult, many theoretical studies of proton transfer reactions have been based on idealized models.[4–6] In a simplified view, proton transfer is often pictured as a one-dimensional process taking place in a double-well potential. Sometimes, important insights can be gleaned even from such one-dimensional treatments.[7,8] An effective barrier height, for example, can be extracted from the splitting of the lowest two energy levels. Nevertheless, theoretical studies based on such simplified low dimensional models do not allow direct comparisons with experimental data. Furthermore, because the motion of the proton is often strongly coupled to the A—A distance, treatments which neglect this coupling are qualitatively in error.[9] It is therefore important to take account of the multidimensional character of the proton-transfer problem.

Unfortunately, it is extremely difficult to treat multidimensional systems quantum mechanically. For a general potential, the cost of the most efficient quantum-mechanical computational methods increases exponentially with the number of degrees of freedom. It is possible to treat six degrees of freedom accurately, but it is very hard to handle larger systems.[10–13] If the form of the potential is specifically chosen to facilitate solving the Schrödinger equation (time-dependent or time-independent), proton transfer problems become more amenable to quantum-computational methods; however, this necessitates imposing an approximate, and necessarily somewhat unrealistic, form on the potential. To avoid imposing an approximate form on the potential, and nonetheless incorporate quantum effects, one can either use Feynman path integral simulations, or mixed quantum-classical methods. In recent years, discretized Feynman path integral simulations have allowed the calculation of statistical equilibrium properties for a variety of large complex quantum-molecular systems.[14,15] For example, the path integral centroid quantum transition state theory suggested by Gillan[16] and by Voth et al.[17,18] can be used to characterize the activation free energy for proton transfer.[19–23] Warshel proposed related approximations that may also be useful.[24,25] However, despite recent progress, this powerful computational approach is not easily extended to calculate time-dependent dynamical properties.[26] A reasonable approach to study dynamical properties of a proton transfer process is to combine quantum and classical mechanics to correctly incorporate the important quantum character of the dynamics of the proton while describing the heavier atoms classically. In this study, we therefore apply and compare mixed quantum-classical computational schemes using a realistic potential to study an intramolecular proton transfer process.

We study the intramolecular proton transfer of the enol form of acetylacetone, whose structure is given in Figure 1. The proton H_a can be bound to either of the two oxygen atoms and the molecule can undergo interconversion between these forms.

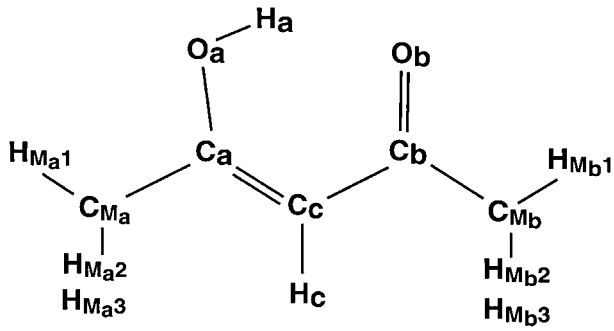

FIGURE 1. The reactant state geometry of acetylacetone.

The potential function is constructed on the basis of the empirical valence bond (EVB) approach of Warshel.[24,27,28] The fact that the reactant and product configurations are mirror images of each other simplifies the construction of a model potential significantly. A more popular molecule for studies of intramolecular proton transfer is malonaldehyde,[9,29–33] which differs from acetylacetone by the absence of the two methyl groups. Malonaldehyde is simpler, but it is not stable in common solvents, whereas acetylacetone is stable in a wide range of polar and nonpolar solvents. The acetylacetone molecule has 15 atoms and a total of 45 degrees of freedom.

In this article we examine the dynamics of the central proton of acetylacetone using two mixed quantum-classical (QC) dynamical methods, a quantum-classical time-dependent self-consistent-field (QC/TDSCF)[34–43] method and a quantum-classical adiabatic method (QC/A)[44–46]. To use the QC/TDSCF method one solves a time-dependent Schrödinger equation for the 3 degrees of freedom of the proton with a potential obtained from the full potential by evaluating it at a classical configuration describing the position of all the other nuclei. The trajectory of the other nuclei in the molecule is determined from classical mechanics using the expectation value of the forces obtained by averaging over the wavepacket associated with the proton. The system is propagated by integrating simultaneously the coupled quantum and classical equations with discrete time-steps. In the classical limit, Newton's equations of motion are recovered by the QC-TDSCF equation. QC/TDSCF can be equivalently formulated in terms of the pure-state density matrix evolution (DME) approach.[42] One obtains the QC/A method if, instead of solving a time-dependent Schrödinger equation for the proton, one assumes that the proton wave function at time t is the instantaneous ground state eigenfunction of the proton Hamiltonian at the classical configuration, $\mathbf{R}(t)$.

Both mixed dynamical methods are approximations to a fully quantum propagation. The QC/A method gives results which are reliable in a well-defined limit. If this limit is realized for the dynamics of a given system, then the mixed-state propagation underlying the QC/TDSCF method should yield results that agree with those from QC/A. However, when there is strong nonadiabatic mixing between the quantum states the QC/A method is non adequate. QC/TDSCF attempts to incorporate the influence of nonadiabadicity in an average way by generating a single mean trajectory. In such cases, the QC/TDSCF results should be more accurate because the QC/A equations may be obtained from the QC/TDSCF equations in the adiabatic limit. The approximation may break down in some cases, however. For example, if the proton wavepacket splits and separates to two distant regions of space, the QC/TDSCF may yield unphysical results, because the classical nuclei are feeling average forces that do not correspond to any well-defined state. Thus, the QC/TDSCF method corresponds to an approximation of unknown validity for long propagation times. Stochastic algorithms have been proposed and used to incorporate nonadiabatic effects by allowing sudden transitions to occur between different adiabatic states (''surface hopping'').[47–50] Nevertheless, for short times, the QC/TDSCF method remains a useful approximation to examine the dynamics of rapid events such as the barrier crossing at the transition state during a proton transfer process. In addition, a comparison of QC/A and QC/TDSCF can be used as a diagnosis to examine the importance of nonadiabatic effects. In particular, such a comparison in the context of a complex molecule described with a realistic potential has never been done.

Even though they are conceptually simple, the QC/A and QC/TDSCF mixed methods have been applied mostly to simplified and highly idealized proton transfer model systems (for QC/TDSCF, see Refs. 40–43; for QC/A, see Refs. 44–46). It is a purpose of the present article to examine the multidimensional dynamics of a proton in the context of a complex molecule described with a realistic potential. Mixed quantum-classical simulations are costly, but will be used more and more frequently as accurate potentials become available. Often, such methods are developed and tested on simple model systems (e.g., the hydrogen motion is restricted to one dimension) and only a small number of excited states are included (e.g., two to four).[40–46,48–50] It is therefore worthwhile exploring the relative merits of the two methods for a realistic potential with a discrete grid representation for the wave function that is able to describe a very large number of excited states. In the next section, we present the details of the methods and the potential energy surface used in our calculation.

Theory and Method

MIXED QUANTUM-CLASSICAL PROPAGATION METHODS

In this section, we present the mixed classical-quantum methods we use. As several groups have used both the QC/TDSCF and the QC/A methods, we merely state the equations and briefly discuss the underlying assumptions.[34–41,44–46]

The fundamental approximation inherent in any TDSCF method is one of separability of the time-dependent wave function. To derive the QC/TDSCF equations one begins by assuming separability of the degrees of freedom to be treated classically and the degrees of freedom to be treated quantum mechanically. In our case, the quantum degrees of freedom are $\mathbf{r} \equiv (x, y, z)$, the three Cartesian components of the proton position, and the classical degrees of freedom are $\mathbf{R} \equiv (X_1, Y_1, Z_1, X_2, Y_2, Z_2, \ldots)$, the Cartesian coordinates of the other atoms in the system. It is assumed that $\psi(\mathbf{r}, \mathbf{R}, t)$, the time-dependent wave function of the entire system, can be approximated by the product $\psi(\mathbf{r}, t)\chi(\mathbf{R}, t)$. Substituting this product ansatz into the Schrödinger equation yields two time-dependent self-consistent Schrödinger equations for the two parts of the total system, each of which contains an effective potential determined by an average over the time-dependent wave function of the other equation. The mixed quantum-classical version of the TDSCF can be obtained by assuming that the wave function $\chi(\mathbf{R}, t)$ is localized about the expectation value of $\mathbf{R}$. If $\chi(\mathbf{R}, t)$ were perfectly localized, the expectation values $\langle \mathbf{R}_i(t) \rangle$ would evolve according to classical equations of motion. Henceforth, we shall not distinguish between the expectation value of the position of the ith classical nucleus $\langle \mathbf{R}_i(t) \rangle$ and $\mathbf{R}_i(t)$, the corresponding classical position.

According to the QC/TDSCF prescription, the proton wave function, $\psi(\mathbf{r}, t)$, obeys the time-dependent Schrödinger equation[34–36]:

$$i\hbar\, \partial_t \psi(\mathbf{r}, t) = \mathscr{H}_\mathrm{p} \psi(\mathbf{r}, t) \tag{1}$$

for the proton Hamiltonian $\mathscr{H}_\mathrm{p}$:

$$\mathscr{H}_\mathrm{p} = \left[-\frac{\hbar^2}{2m}\nabla^2 + V(\mathbf{r}, \mathbf{R}(t)) \right] \tag{2}$$

where m is the mass of the proton and $V(\mathbf{r}, \mathbf{R}(t))$ is the potential energy. The position of the ith nucleus obeys the classical equation of motion:

$$M_i \ddot{\mathbf{R}}_i(t) = \int d^3\mathbf{r}\, \psi^*(\mathbf{r}, t) \mathscr{F}_i(\mathbf{r}, \mathbf{R}(t)) \psi(\mathbf{r}, t) \tag{3}$$

where M_i is the mass of the nucleus and $\mathscr{F}_i(\mathbf{r}, \mathbf{R}(t)) = -\partial V(\mathbf{r}, \mathbf{R})/\partial \mathbf{R}_i$, evaluated with the classical nuclei at their position $\mathbf{R}(t)$.

We have also implemented a mixed quantum-classical method based on an adiabatic approximation (QC/A).[44–46] One can imagine at least two ways of deriving the QC/A equations. One way is to start from the QC/TDSCF and make an adiabatic approximation to solve the time-dependent Schrödinger equation [eq. (1)]. For this purpose, one considers the expansion of $\psi(\mathbf{r}, t)$:

$$\psi(\mathbf{r}, t) = \sum_n c_n(t) \phi_n(\mathbf{r}; \mathbf{R}(t)) e^{-i\int_0^t \varepsilon_n(t')dt'/\hbar} \tag{4}$$

in terms of the instantaneous eigenfunctions $\phi_n(\mathbf{r}, \mathbf{R}(t))$ of the proton Hamiltonian $\mathscr{H}_\mathrm{p}$:

$$\mathscr{H}_\mathrm{p} \phi_n(\mathbf{r}, \mathbf{R}(t)) = \varepsilon_n(\mathbf{R}(t)) \phi_n(\mathbf{r}, \mathbf{R}(t)) \tag{5}$$

If the system is adiabatic so that:

$$\langle \phi_n | \partial_t V | \phi_m \rangle \ll \frac{1}{\hbar} [\, \varepsilon_n(\mathbf{R}(t)) - \varepsilon_m(\mathbf{R}(t))]^2 \tag{6}$$

then (see Ref. 51) $\partial_t c_n(t) \sim 0$, and if the wavepacket is $\phi_0(\mathbf{r}; \mathbf{R}(0))$ at time $t = 0$ then $c_n(t) \approx c_n(t = 0) = \delta_{n0}$. According to the adiabatic approximation the proton wave function adapts instantaneously to the movement of the classical atoms, and is always equal to the ground state of the proton potential determined by the position of the classical atoms at time t. In this case, the classical equation for the motion of the heavier atoms becomes:

$$M_i \ddot{\mathbf{R}}_i(t) = \int d\mathbf{r}\, \phi_0^*(\mathbf{r}; \mathbf{R}(t)) \mathscr{F}_i(\mathbf{r}, \mathbf{R}(t)) \phi_0(\mathbf{r}, \mathbf{R}(t)) = -\frac{\partial \varepsilon_0(\mathbf{R}(t))}{\partial \mathbf{R}_i} \tag{7}$$

where the last equality follows from the Hellmann–Feynman theorem.

Another way to derive the QC/A equations, which offers a different perspective and does not directly invoke the TDSCF approximation, is to

represent the time-dependent Schrödinger equation for the entire system:

$$[T_c + \mathscr{H}_p]\Psi(\mathbf{r}, \mathbf{R}, t) = i\hbar\, \partial_t \Psi(\mathbf{r}, \mathbf{R}, t) \qquad (8)$$

where T_c is the kinetic energy operator of the classical particles, in the $\phi_n(\mathbf{r}; \mathbf{R})$ basis;

$$\sum_m \langle \phi_n(\mathbf{r}; \mathbf{R}) | [T_c + \mathscr{H}_p] | \phi_m(\mathbf{r}; \mathbf{R}) \rangle \times \langle \phi_m(\mathbf{r}; \mathbf{R}) \,|\, \Psi(\mathbf{r}, \mathbf{R}, t) \rangle = i\hbar\, \partial_t \langle \phi_n(\mathbf{r}; \mathbf{R}) \Psi(\mathbf{r}, \mathbf{R}, t) \rangle \qquad (9)$$

If one neglects nonadiabatic coupling, $\langle \phi_m(\mathbf{r}; \mathbf{R}) | T_c | \phi_n(\mathbf{r}; \mathbf{R}) \rangle$, this becomes (for the ground state):

$$[T_c + \varepsilon_0(\mathbf{R})]\theta_0(\mathbf{R}, t) = i\hbar\, \partial_t \theta_0(\mathbf{R}, t) \qquad (10)$$

where:

$$\theta_0(\mathbf{R}, t) = \langle \phi_0(\mathbf{r}; \mathbf{R}) \,|\, \Psi(\mathbf{r}, \mathbf{R}, t) \rangle \qquad (11)$$

In effect, the **R** nuclei move on an effective potential, $\varepsilon_0(\mathbf{R})$, corresponding to the configuration-dependent proton ground state energy. In the classical limit, eq. (10) is replaced by eq. (7).

Clearly, one obtains the same QC/A equations using either the first or the second route. In the first derivation, one begins from the QC/TDSCF result (i.e., assuming separability of the classical and quantum degrees of freedom), takes the classical limit, and finally makes an adiabatic approximation. In the second derivation, one begins from the time-dependent Schrödinger equation for the entire system, makes an adiabatic approximation, and finally makes a classical approximation. In particular, the product ansatz is never explicitly invoked in the derivation. The first derivation shows that the QC/TDSCF and the QC/A methods should give very similar results if the adiabatic approximation is good. If one did not wish to approximate the motion of the heavier nuclei with classical mechanics, one could still derive an adiabatic approximation by following the second derivation. This would not be possible with the first derivation, because it is built upon the QC/TDSCF equations, which include the classical approximation.

Although the QC/TDSCF and the QC/A approximations are different, the implementation of the two mixed quantum-classical methods is, in practice, very similar. The quantum part of the QC/TDSCF method implicates a time-dependent Schrödinger [eq. (1)] and $\psi(\mathbf{r}, t)$ is a function of time, whereas the quantum part of the QC/A method implicates a time-independent Schrödinger equation [eq, (5)] and the $\phi_0(\mathbf{r}; \mathbf{R}(t))$ depends parametrically on time. In both cases, the forces on the classical particles are computed from an average over the proton wave function [using $\psi(\mathbf{r}, t)$ in QC/TDSCF and $\phi_0(\mathbf{r}; \mathbf{R}(t)$ in QC/A]. According to eq. (6), if the initial quantum wavepacket for the QC/TDSCF propagation is chosen to be the ground state $\phi_0(\mathbf{r}; \mathbf{R}(0))$, the solution of the time-independent Schrödinger equation [eq. (5)], then the QC/TDSCF and QC/A methods should give very similar results as long as the energy difference between the ground and the lowest excited states of the proton is large enough to prevent significant population of the latter. The QC/TDSCF allows the proton to occupy any combination of eigenstate $\phi_n(\mathbf{r}; \mathbf{R}(t))$, whereas the QC/A restricts the proton wave function to $\phi_0(\mathbf{r}; \mathbf{R}(t))$. The QC/TDSCF method incorporates nonadiabatic effects not present in the QC/A method. Nonadiabatic coupling effects could also be included in a mixed quantum-classical method by allowing transitions between the different adiabatic eigenstates ϕ_n using a surface-hopping model.[48–50] In Tully's "fewest switch surface hopping algorithm,"[48,49] the full coherence of the wave function $\psi(\mathbf{r}, t)$ is retained, as in eq. (1), while the classical nuclei move according to forces determined from the nth adiabatic state $\phi_n(\mathbf{r}; \mathbf{R}(t))$. A Monte Carlo process is used to introduce abrupt transitions between the various adiabatic states and the dynamics has a stochastic character. In QC/TDSCF, the classical nuclei move via eq. (3) according to the average forces and the result is a single mean trajectory.

POTENTIAL ENERGY SURFACE

To study the proton transfer of acetylacetone we require an accurate potential energy surface which allows the proton to move from one oxygen atom to the other. On the other hand, because the potential is evaluated many times, it should be simple. The most rigorous potential energy surfaces are obtained directly from *ab initio* calculations, but it is computationally prohibitive to use *ab initio* potentials in mixed quantum-classical molecular dynamics, which requires the repeated evaluation of the potential energy $V(\mathbf{r}, \mathbf{R})$ and forces $\mathscr{F}_i(\mathbf{r}, \mathbf{R})$ at a large number of points in **r** space to permit evaluation of the integrals in eqs. (3) and (7). To devise a

practical model, an empirical potential energy surface was constructed and its parameters were fitted to reproduce key results of *ab initio* calculations. The model is described in detail in Ref. 52.

The model uses the empirical valence bond (EVB) approach to Warshel[24,27,28] to combine a potential energy function for the reactant, V_1, and a potential energy function for the product, V_2, into a total potential energy surface that allows a transition between these two geometries. The EVB potential is defined as the lower eigenvalue of an effective ''Hamiltonian'' of a two-state system whose diagonal elements are V_1 and V_2 and whose off-diagonal element ϵ is constant:

$$V(V_1, V_2, \epsilon) = \frac{V_1 + V_2}{2} - \left[\left(\frac{V_1 + V_2}{2}\right)^2 - V_1V_2 + \epsilon^2\right]^{1/2} \quad (12)$$

The EVB potential V is a multidimensional double-well potential with reactant and product wells which are similar (but not identical) to the wells of V_1 and V_2 and a barrier between the wells whose height is controlled by the coupling parameter ϵ, the value of which must be found as part of a fitting procedure. The reactant and product potentials V_1 and V_2 consist mostly of standard bond, angle, dihedral, and nonbonded potentials; we use the CHARMM potential,[53] in which the bond and angle potentials are harmonic, the dihedral potentials consist of a single cosine term, and the nonbonded interactions contain both a Coulomb and a Lennard–Jones contribution. To reproduce the significant anharmonicity observed in the *ab initio* potential energy surface, the O—H bonds were described by a Lennard-Jones type potential. All other bonds were represented by harmonic functions.

The parameters of the empirical model were fitted to key features of an *ab initio* potential energy surface with points calculated at the HF/4-31G* and HF/6-31G* levels of theory using GAUSSIAN-90.[54] The features used as fitting criteria are: (1) the reactant and product geometries; (2) the energy barrier between the reactant (or product) geometry and transition state geometry; (3) the electrostatic potential surface around the molecule; (4) the energy as a function of torsional deformation from the reactant geometry; and (5) the potential energy surface for the transferring proton with all other atoms fixed in the reactant or in the transition state geometries.

Details about the construction of this potential energy model and a list of the values of all parameters can be found in Ref. 52.

CALCULATIONS

To implement the QC/TDSCF method we solve eq. (1) by applying the split operator technique [55]:

$$\psi(\mathbf{r}, t + \tau_q) = \exp\left[-iV(\mathbf{r}, \mathbf{R}(t))\frac{\tau_q}{2\hbar}\right] \times \exp\left[+i\frac{\tau_q\hbar}{2m}\nabla^2\right] \times \exp\left[-iV(\mathbf{r}, \mathbf{R}(t))\frac{\tau_q}{2\hbar}\right]\psi(\mathbf{r}, t) \quad (13)$$

where τ_q is the (quantum) time step and $V(\mathbf{r}, \mathbf{R}(t))$ is the potential, which is a function of $\mathbf{r}$ for a given classical configuration $\mathbf{R}(t)$ at time t. The wavepacket is represented on a three-dimensional Cartesian grid. The potential energy operator is applied directly in real space. The kinetic energy operator is applied by transforming to a basis of products of plane waves using a three-dimensional fast Fourier transform (3D-FFT).[10,56]

To implement the QC/A method, we calculate $\phi_0(\mathbf{r}; \mathbf{R}(t))$ using a relaxation procedure by propagating the Schrödinger equation in imaginary time.[57] Again, the propagation is done with the split operator technique: at each classical configuration $\mathbf{R}(t)$, we repeatedly use eq. (13) with an imaginary time step, $\tau_q \rightarrow i\tau_q$, to relax to the ground state, maintaining the normalization of the wave function.

For both methods, the classical degrees of freedom were propagated with a classical time step τ_c using a variant of the Verlet algorithm[58]:

$$\mathbf{R}_i(t + \tau_c) = 2\mathbf{R}_i(t) - \mathbf{R}_i(t - \tau_c) + \frac{\tau_c^2}{M_i}\mathbf{F}_i(t) + O\left[(\tau_c)^4\right] \quad (14)$$

as implemented in the molecular dynamics package CHARMM.[53] This algorithm was also used for

the purely classical simulations that we performed for comparison.

The QC/TDSCF simulations were started with an initial wavepacket $\psi(\mathbf{r}, t = 0)$ and an initial classical configuration $\mathbf{R}(t = 0)$. The QC/A simulations were started with an initial classical configuration $\mathbf{R}(t = 0)$. The simulations were performed by executing the following steps:

(i) Evaluate the potential $V(\mathbf{r}, \mathbf{R}(t))$ and the forces $\mathcal{F}_i(\mathbf{r}, \mathbf{R}(t))$ at all points $\mathbf{r}$ for the classical configuration $\mathbf{R}(t)$.

(ii) Calculate the average forces $\langle \mathcal{F}_i \rangle$ on the classical particles using either $\psi(\mathbf{r}, t)$ (QC/TDSCF) or $\phi_0(\mathbf{r}; \mathbf{R}(t))$ (QC/A).

(iii) Generate a classical dynamical step with eq. (14) to compute the next classical configuration $\mathbf{R}(t + \tau_c)$ using the average forces $\langle \mathcal{F}_i \rangle$.

(iv) Using the potential $V(\mathbf{r}, \mathbf{R}(t))$, compute the next wave function, $\psi(\mathbf{r}, t + \tau_c)$, with the split operator technique with real-time propagation (QC/TDSCF) or the next ground state $\phi_0(\mathbf{r}; \mathbf{R}(t + \tau_c)$ by relaxation using the split operator technique with imaginary time propagation (QC/A).

(v) With the new classical configuration $R(t + \tau_c)$ and the new $\psi(\mathbf{r}, t + \tau_c)$ (QC/ TDSCF), or the new $\phi_0(\mathbf{r}; \mathbf{R}(t + \tau_c)$ (QC/ A) at time $t + \tau_c$, repeat the above steps.

Two initial configurations of the classical atoms were considered, the reactant and transition state configurations. Classical, QC/TDSCF, and QC/A trajectories were generated for both initial configurations for a total of six trajectories. The reactant configuration is the absolute minimum of the potential energy surface for this molecule; the transition state configuration is the saddle point between the reactant and product configuration. The geometries are given in Ref. 52. To directly compare the simulations started at the reaction or transition configurations, exactly the same initial positions and velocities were used for the classical atoms for both the QC/TDSCF and the QC/A, and the QC/TDSCF initial proton wavepacket was chosen as the ground state wave function corresponding to the configuration of the classical nuclei. The ground state was obtained by starting with a Gaussian wavepacket centered in the deepest proton energy well for the fixed configuration of the classical nuclei (reactant or transition state) and then using the imaginary time relaxation method[57] to relax to the ground state. When the classical atoms are fixed at their transition state configuration positions the proton potential has a single well and, therefore, the initial wave function is localized. The initial velocities of the classical atoms were taken from a Boltzmann distribution at a temperature of 300 K and chosen such that the center-of-mass velocity of the total system was zero. The simulations were performed for a total time of 0.5 ps. A time step of 1 fs was used in the numerical integration of the classical equations. Because the wavepacket propagation requires a smaller time step than the classical trajectory calculation, we used a smaller time step in eq. (13) than in eq. (14): $\tau_c = 12\tau_q$. That is, for each classical integration time step, we performed 12 quantum time steps. The same quantum time step was used to propagate the QC/TDSCF time-dependent Schrödinger equation for the proton and to solve the time-dependent Schrödinger equation for the eigenstates of the proton.

The wave functions were represented on a grid extending from -1.5 Å to $+1.5$ Å with the center at the minimum of the proton potential corresponding to the initial classical configurations. The number of grid points was increased until convergence was obtained with 32 points along each proton degree of freedom. There were a total of $32 \times 32 \times 32 = 32{,}768$ plane wave basis functions or grid points. To verify that the density of grid points was high enough, we increased the size of the grid from 3 to 3.5 Å, keeping the same number of grid points, and found that the average bond lengths (see Figs. 2 and 3) did not change by more than 2% and that the average kinetic energy (see Fig. 5) did not change by more than 10%. Because increasing the size of the grid from 3 to 3.5 Å caused a drastic change in the density of points our results are converged to within less than 2% (bond lengths) and 10% (kinetic energy). To facilitate the propagation we used a potential ceiling at $V = 100$ kcal/mol above the energy of the reactant geometry, which is the absolute minimum of the potential energy surface. The value of the ceiling must be chosen high enough to both compute the ground state of the proton and to propagate the QC/TDSCF wavepacket accurately. Increasing its value did not change our results. We have also confirmed that our quantum and classical time

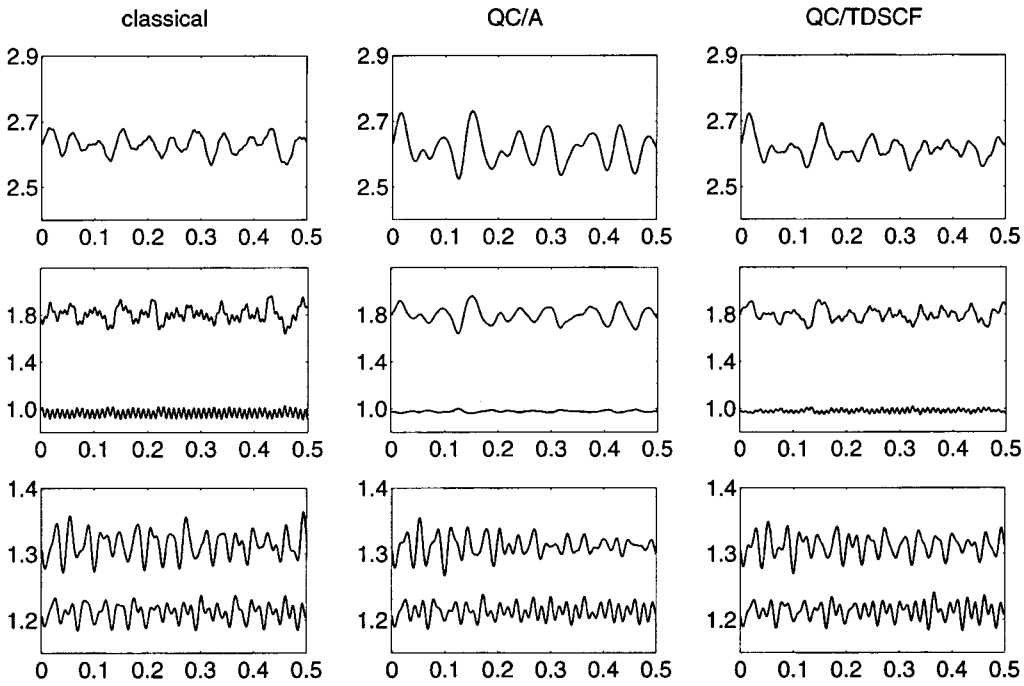

FIGURE 2. Geometric data as a function of time, taken from the trajectories starting from the reactant configuration. The first row of panels shows the O_a—O_b distance, the second row the O_a—H_a and O_b—H_a distances, and the third row the O_a—C_a and O_b—C_b distances. The columns of panels are, from left to right, the classical, adiabatic, and QC/TDSCF results. Time is indicated in ps.

steps are small enough to assure correct propagation; that is, decreasing them does not change the trajectories significantly.

To calculate the proton ground state wave function with the imaginary time relaxation method, we used a convergence criterion of $|\langle V\rangle_{n+1} - \langle V\rangle_n| \leq 1.0 \times 10^{-10}$ hartrees, where $\langle V\rangle_n$ is the average potential for the nth iteration of the relaxation process. We found that it was critical to impose such a strict convergence criterion to obtain conservation of energy throughout the adiabatic simulations. Using this criterion, the number of relaxation iterations required to converge to the ground state, per geometry of the classical atoms, was as large as 400. To calculate the ground state wave function at time $t + \tau_c$ we began the iteration with the ground state wave function at time t. Difficulties in realizing conservation of energy in QC/A propagation have been discussed previously in the context of the dynamics of the solvated electron.[59]

The CPU times, on a 40-MHz R3000 SGI machine, were about 50 and 140 hours for each QC/TDSCF and QC/A simulation, respectively. Most of this time was spent evaluating the energy and forces at each of the 32,768 grid points needed for the proton wave function.

Results and Discussion

We first compare the trajectories obtained from the different methods. Figures 2 and 3 show several bond distances obtained from the classical, QC/TDSCF and QC/A calculations starting from the reactant and transition geometries, respectively. For the QC/TDSCF and QC/A simulations, the O—H distance is calculated as $\langle r_{O-H}(t)\rangle$, averaging over the proton wave function. For the trajectories starting from the reactant configuration (Fig. 2), the classical, QC/TDSCF, and QC/A calculations all give very similar results. It appears, however, that at least for the O_a—H_a, O_b—H_a, and O_a—O_b bonds, the classical calculation yields bond lengths that oscillate more rapidly than their QC/TDSCF counterparts, which in turn oscillate more quickly than the corresponding QC/A bond lengths. This probably indicates that energy flow is

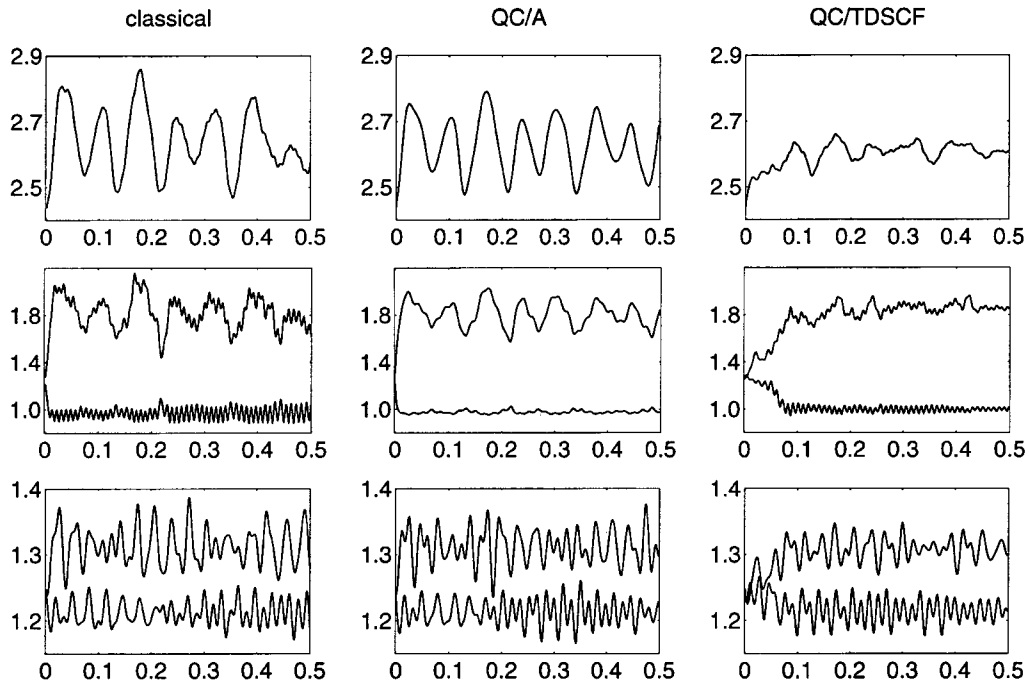

FIGURE 3. Same as Figure 2 except for the trajectories starting from the transition state configuration. Time is indicated in ps.

less constrained in the classical than in the QC/TDSCF simulation and less constrained in the QC/TDSCF simulation than in the adiabatic simulation.

For the transition state trajectory the O_a—H_a, O_b—H_a, and O_a—O_b bond length from QC/TDSCF and QC/A are noticeably different. The average bond lengths computed with the QC/A method change more abruptly than their QC/TDSCF counterparts because of the nature of the time dependence of the proton wave function. For both the QC/A and the QC/TDSCF trajectory, the proton wave function is chosen to be the ground state at $t = 0$. Because the proton's potential has a single well when the classical atoms assume their positions at the transition state configuration, the initial wave function is localized. During the trajectory, the QC/A wave function adapts instantaneously to the configuration of the classical atoms. The wave function remains localized as we propagate and simply falls into a well because its position at time $t + \tau$ depends only on the values of the potential at time $t + \tau$ and not on its position (or the potential) at time t. The evolution of the QC/A proton wave function has thus no memory of its past, which corresponds to a total absence of inertial dynamical effects. This is not true of the QC/TDSCF trajectory. The position of the QC/TDSCF wavepacket at time $t + \tau$ depends not only on the potential at time $t + \tau$ but also on the wavepacket at time t, which results in a certain inertia in the dynamics of the proton wavepacket. The evolution of the QC/A and the QC/TDSCF wavepackets for the trajectory initiated at the transition state is shown in Figure 4. It can be seen that the adiabatic ground state is always localized near the deepest minimum, whereas the position of the QC/TDSCF wavepacket can stray from the minimum (this is most clearly visible at 120 fs). This is a consequence of the QC/TDSCF wavepacket's dependence on its previous position.

The two mixed quantum-classical methods yield different configurational properties during the trajectories (proton position, bond lengths, etc.) due to the influence of inertial effects. In addition, there are also important differences in the dynamical properties. For example, as shown in Figure 5, the average proton kinetic energy is much higher for the QC/TDSCF simulation than for the adiabatic simulation. This is consistent with the observation that the values of the wave vector $\mathbf{k}$, which contribute to the QC/TDSCF wavepacket, are larger than the values that contribute to the proton ground state wave function and that the QC/TDSCF wave function has more spatial oscillations

(see Fig. 4). Due to the neglect of inertial effects, the proton does not need to dissipate kinetic energy as it falls into the energy well during the QC/A trajectory. In contrast, inertial effects during the QC/TDSCF trajectory result in a higher kinetic energy. On the other hand, there is almost no noticeable difference in the two types of propagation for the trajectory initiated in the reactant configuration because the QC/A and the QC/TDSCF wave functions behave very similarly in that case. The reason is that the potential felt by the proton is always a single well potential and does not change much with time. Nevertheless, it should be emphasized that the ultimate fate of the classical, QC/A, and QC/TDSCF trajectories, initiated at the transition state, is the same.

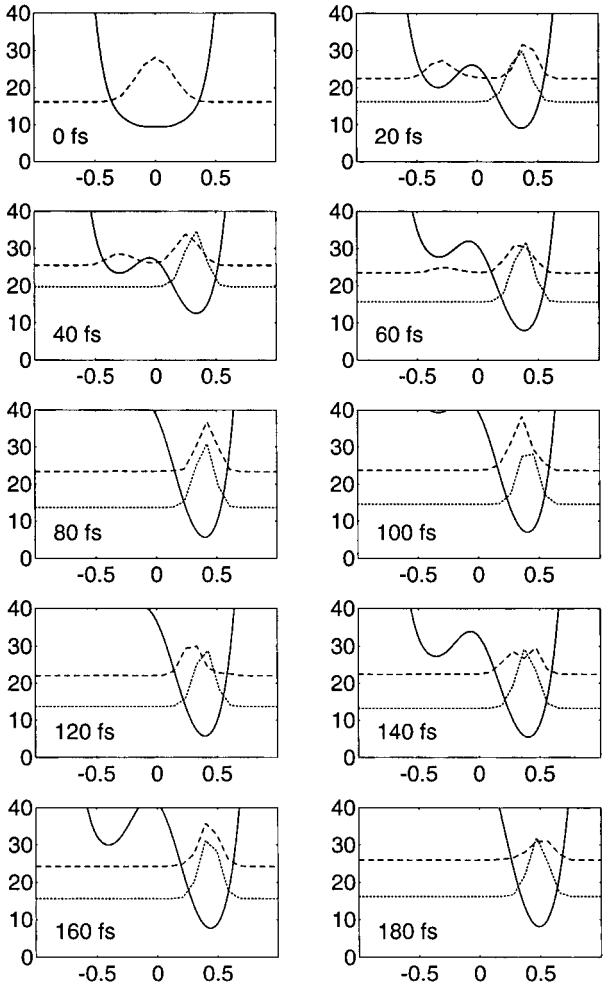

FIGURE 4. A one-dimensional cut through the proton potential energy surface (solid curve), the SCF proton density (dashed curve), and the ground state proton density corresponding to the potential energy surface (dotted curve) for several configurations along the QC/TDSCF trajectory starting from the transition state. The time interval between consecutive snapshots is 20 fs. The first snapshot represents the starting configuration; the single proton density profile shown represents the ground state. The line along which the values are given is parallel to the O_a—O_b axis and passes through the mean value of the proton position. The zero point on this line is defined by the projection of the midpoint between O_a and O_b onto this line. The proton densities have been scaled arbitrarily (but identically), and their baselines indicate the energy of the corresponding wavepacket. (See also Fig. 6.)

For the transition state trajectories, the QC/A method appears to be clearly inadequate. During the QC/A trajectories the average proton position varies too rapidly because the proton wave function reacts instantaneously to the configuration of the classical atoms. In effect, the rapid time variation of the proton potential energy surface near the transition state causes a breakdown of the adiabatic approximation expressed by eq. (6). As is clear from the first derivation of the QC/A equations presented above, the QC/A method cannot be better, and in fact must be worse than the QC/TDSCF results, because one must make an additional approximation to obtain the QC/A equations from the QC/TDSCF equations. Although we do not claim to have implemented either method in the most efficient manner possible, we note that our QC/A calculations are much more costly than the QC/TDSCF calculations. The QC/A calculation is more costly, because, to conserve energy during the propagation, we needed to converge the instantaneous ground states very accurately.

An important question remains: Should one expect the QC/TDSCF approximation to be accurate for our proton transfer problem? It is clear that the QC/TDSCF approximation will be good if the effect of the coupling between the **r** and the **R** degrees of freedom is well represented by average potentials. In general, the approximation will be poor if the **r** degree of freedom wavepacket bifurcates. Although our proton wavepacket is generally localized about a single point, sometimes the proton wavepacket does briefly separate into two parts. Such a bifurcation is shown in Figure 6. When bifurcations occur, a trajectory determined from a mean force might not represent the true dynamics. However, even if the proton wavepacket does separate into two parts, the QC/TDSCF approximation should be good if either: (i) the position of the classical nuclei does not depend sensitively on the proton wavepacket (i.e., the coupling is very weak); or (ii) the motion of the proton is

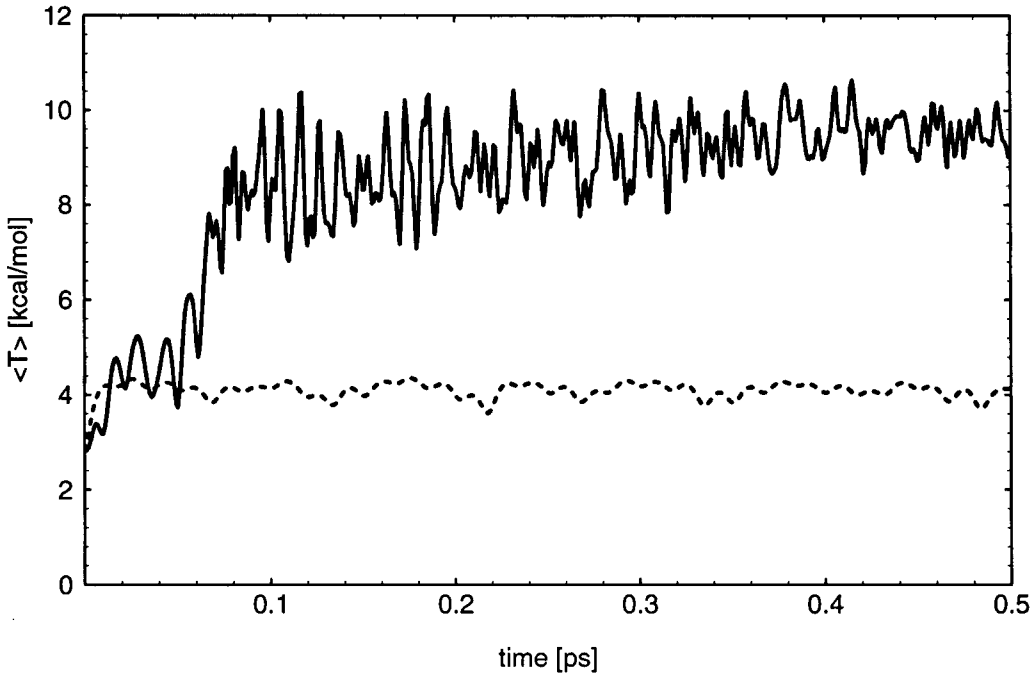

FIGURE 5. The average kinetic energy, $\langle T \rangle$, for the transition state trajectory as a function of time from the QC/TDSCF (solid line) and adiabatic (dashed line) simulations.

fast relative to the response time of the classical nuclei. The sensitivity of the trajectory of the classical atoms to an occasional and brief bifurcation of duration Δt will depend on the magnitude of the resulting uncertainty in the impulse, $\Delta \mathscr{F}_{\mathrm{rms}} \Delta t$, relative to the net impulse $\langle \mathscr{F} \rangle \Delta t$ caused by the average force and the net momentum **P**. Thus, we expect the QC/TDSCF approximation to remain quite good for simulations at 300 K, despite occasional splitting of the proton wavepacket, because the proton motion is fast enough that the motion of the classical nuclei is strongly determined by the average potential irrespective of the bifurcation. In the tunnelling regime this would not be true: the motion of the proton would not be fast enough to compensate for bifurcation of the wavepacket. Where QC/TDSCF is insufficient one might resort to stochastic surface-hopping algorithms[48–50] or multiconfiguration TDSCF.[60–62]

Conclusion

Initial results of a mixed quantum-classical molecular dynamics study of acetylacetone have been presented. Two quantum-classical dynamical propagation methods were used, QC/TDSCF and QC/A. Trajectories were run on a realistic multidimensional potential energy surface fitted to *ab initio* properties of the acetylacetone molecule. The three quantum degrees of freedom of the proton were treated quantum mechanically and the remaining 42 degrees of freedom were treated classically. Although such computational approaches have been used previously by others in various contexts,[39–46] it is the first time, to our knowledge, that the QC/TDSCF and QC/A methods have been applied to study the multidimensional dynamics of a proton in a complex molecule using a realistic potential (of course, proton transfers in multidimensional systems have been investigated previously using other approaches; see for example Refs. 19–25). For classical initial velocities chosen from a Boltzmann distribution at 300 K the results of classical, QC/TDSCF, and adiabatic calculations were compared. We find that the time-dependent QC/TDSCF wavepacket, $\psi(\mathbf{r}, t)$, and the adiabatic ground state of the proton, $\phi_0(\mathbf{r}; R(t))$, sometimes behave rather differently. The position of the adiabatic ground state depends on the position of the deepest minimum of the proton potential. If the classical atoms move so as to create a potential for the proton with one deep minimum, then the proton ground state wave function imme-

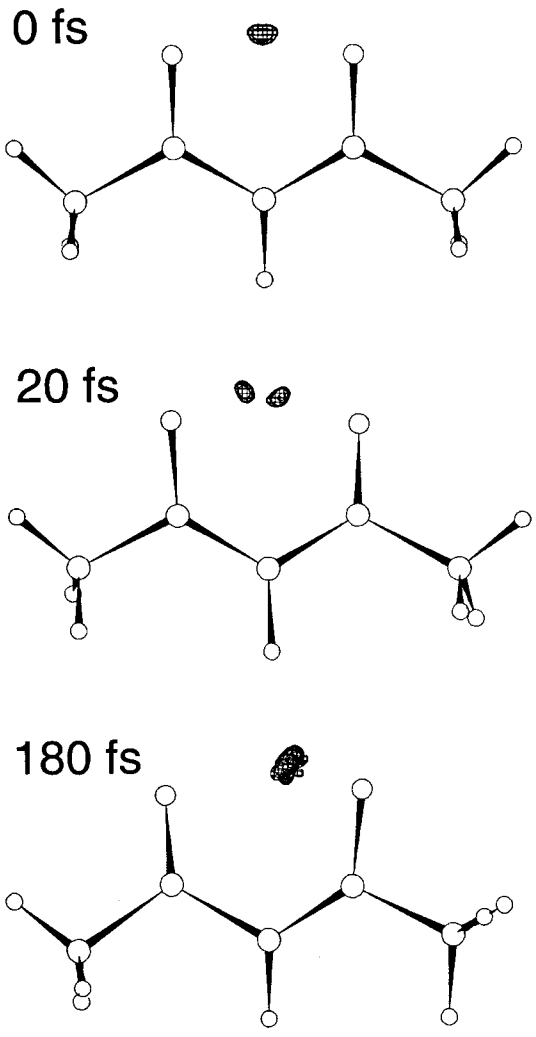

FIGURE 6. Three-dimensional density plot of the QC/TDSCF wave function superimposed on the molecule at 0, 20, and 180 fs along the transition state trajectory.

diately moves so that it sits over this minimum. The position of the QC/TDSCF wavepacket at time $t + \tau$ depends not only on the potential the proton feels at time $t + \tau$, but also on where the wavepacket was at time t. If the configuration of the classical atoms changes very slowly, the position of the proton ground state will move slowly and it will be more consistent with the QC/TDSCF wavepacket.

As we discussed, although the quantum-mechanical adiabatic equations are not obtained from the quantum-mechanical TDSCF equations by introducing an adiabatic approximation, the working equations of the QC/A method *are* obtained from their QC/TDSCF counterparts by making an adiabatic approximation [see eq. (6)]. This obviously means that the QC/TDSCF results are always more accurate than the QC/A results. Although both methods are approximate one can assess the importance of nonadiabatic coupling by comparing the QC/TDSCF and the QC/A results. Differences between our QC/TDSCF and our QC/A results are a measure of the importance of nonadiabatic coupling. It is important to study the difference between QC/A and QC/TDSCF for a realistic potential. We have observed important differences for a realistic (multidimensional) acetylacetone potential. As we implement them, the QC/TDSCF method is also more computationally efficient than the QC/A method. Due to the apparent importance of the nonadiabatic coupling, and the relative inefficiency of the QC/A method, we therefore recommend the QC/TDSCF over the QC/A approach.

Simulations of the kind we have performed are too short to actually observe a net proton transfer. The QC/A and QC/TDSCF trajectories do not provide an effective sampling of transfer events for cases with a non-negligible activation barrier. However, the present calculations are only the first stage of investigations of the dynamics of proton transfer in acetylacetone. In the future, we will generate an ensemble of activated trajectories initiated near the transition state. Such calculations will enable us to calculate the proton transfer rate constant and provide invaluable information concerning important recrossing events at the transition state. To calculate the rate constant it is obviously necessary to develop and understand the limitations of methods for solving the dynamics. In addition, the influence of solvent molecules during the proton transfer reaction could be investigated by performing simulations of acetylacetone in polar and nonpolar solvents. Finally, because there simulations will be CPU intensive, it will be worthwhile to explore the possibility of accelerating the calculations by optimizing the proton grid, improving the propagation algorithm, and reducing the number of times the potential is evaluated.

Acknowledgments

B. Roux is a MRC research fellow. This work was supported by grants from FCAR (Quebec) and NSERC (Canada).

References

1. S. Scheiner, *Acc. Chem. Res.*, **18**, 174 (1985).
2. R. P. Bell, *The Proton in Chemistry*, Chapman & Hall, London, 1973.
3. D. Borgis, *Electron and Proton Transfer Processes in Chemistry and Biochemistry*. Elsevier, New York, 1991.
4. D. Borgis and J. T. Hynes, *Chem. Phys.*, **170**, 315 (1993).
5. A. Suáez and R. Silbey, *J. Chem. Phys.*, **94**, 4809 (1991).
6. J. Lobaugh and G. A. Voth, *J. Chem. Phys.*, **100**, 3039 (1993).
7. H.-H. Limbach and J. Hennig, *J. Chem. Phys.*, **71**, 3120 (1979).
8. Y. Tomioka, M. Ito, and N. Mikami, *J. Phys. Chem.*, **87**, 4401 (1983).
9. T. Carrington, Jr. and W. H. Miller, *J. Chem. Phys.*, **84**, 4364 (1986).
10. R. Kosloff, *J. Phys. Chem.*, **92**, 2087 (1988).
11. S. Carter and N. C. Handy, *Comp. Phys. Rep.*, **5**, 115 (1986).
12. J. Tennyson, S. Miller, and J. R. Henerson, *Methods in Computational Chemistry*, Vol. 4, Plenum Press, New York, 1992.
13. M. J. Bramley and T. Carrington, *J. Chem. Phys.*, **99**, 8519 (1993).
14. R. P. Feynman and A. R. Hibbs, *Quantum Mechanics and Path Integrals*, McGraw-Hill, New York, 1965.
15. D. Chandler, In *Liquides, Cristallisation et Transition Vitreuse, Les Houches, Session LI*, D. Levesque, J.-P. Hansen, and J. Zinn-Justin, Eds., Elsevier, New York, 1991.
16. M. J. Gillan, *J. Phys. C*, **20**, 3621 (1987).
17. G. A. Voth, D. Chandler, and W. H. Miller, *J. Chem. Phys.*, **91**, 7749 (1989).
18. G. A. Voth, *J. Phys. Chem.*, **97**, 8365 (1993).
19. J.-K. Hwang and A. Warshel, *J. Phys. Chem.*, **97**, 10053 (1993).
20. H. Azzouz and D. Borgis, *J. Chem. Phys.*, **98**, 7361 (1993).
21. D. Laria, G. Ciccotti, M. Ferrario, and R. Kapral, *Chem. Phys.*, **180**, 181 (1994).
22. S. Consta and R. Kapral, *J. Chem. Phys.*, **101**, 10908 (1994).
23. K. Hinsen and B. Roux, *J. Chem. Phys.*, **106**, 3567 (1997).
24. A. Warshel, *J. Phys. Chem.*, **86**, 2218 (1981).
25. A. Warshel and Z. T. Chu, *J. Chem. Phys.*, **93**, 4003 (1990).
26. J. Cao and G. A. Voth, *J. Chem. Phys.*, **101**, 6157 (1994).
27. A. Warshel and R. M. Weiss, *J. Am. Chem. Soc.*, **102**, 6218 (1980).
28. Y.-T. Chang and W. H. Miller, *J. Phys. Chem.*, **94**, 5884 (1990).
29. S. Takada and H. Nakamura, *J. Chem. Phys.*, **100**, 98 (1994).
30. Y. Guo, T. D. Sewell, and D. L. Thompson, *Chem. Phys. Lett.*, **224**, 470 (1994).
31. Z. Smedarchina, W. Siebrand, and M. Z. Zgierski, *J. Chem. Phys.*, **103**, 5326 (1995).
32. N. Shida, P. F. Barbara, and J. E. Almlöf, *J. Chem. Phys.*, **91**, 4061 (1989).
33. E. Bosch, M. Moreno, J. M. Lluch, and J. Bertrán, *J. Chem. Phys.*, **93**, 5865 (1990).
34. R. B. Gerber and M. A. Ratner, *Adv. Chem. Phys.*, **70**, 97 (1988).
35. R. B. Gerber and R. Alimi, *Israel J. Chem.*, **31**, 383 (1991).
36. R. Alimi, R. B. Gerber, A. D. Hammeric, R. Kosloff, and M. A. Ratner, *J. Chem. Phys.*, **93**, 6484 (1990).
37. G. D. Billing, *Comp. Phys. Rep.*, **12**, 383 (1990).
38. G. D. Billing, *Chem. Phys.*, **70**, 223 (1982).
39. K. Haug and H. Metiu, *J. Chem. Phys.*, **99**, 6253 (1993).
40. P. Bala, B. Lesyng, and J. A. McCammon, *Chem. Phys.*, **180**, 271 (1994).
41. P. Bala, B. Lesyng, and J. A. McCammon, *Chem. Phys. Lett.*, **219**, 259 (1994).
42. H. J. C. Berendsen and J. Mavri, *J. Chem. Phys.*, **97**, 13464 (1993).
43. J. Mavri, H. J. C. Berendsen, and W. F. van Gunsteren, *J. Chem. Phys.*, **97**, 13469 (1993).
44. D. Laria, G. Ciccotti, M. Ferrario, and R. Kapral, *J. Chem. Phys.*, **97**, 378 (1992).
45. D. Borgis, G. Tarjus, and H. Azzouz, *J. Chem. Phys.*, **96**, 3188 (1992).
46. D. Borgis, G. Tarjus, and H. Azzouz, *J. Chem. Phys.*, **97**, 1390 (1992).
47. A. Warshel and J.-K. Hwang, *J. Chem. Phys.*, **84**, 4938 (1986).
48. S. Hammes-Schiffer and J. C. Tully, *J. Chem. Phys.*, **101**, 4657 (1994).
49. S. Hammes-Schiffer and J. C. Tully, *J. Chem. Phys.*, **103**, 8528 (1995).
50. S. Consta and R. Kapral, *J. Chem. Phys.*, **104**, 4581 (1996).
51. D. ter Haar, *Problems in Quantum Mechanics*, Pion, London, 1975.
52. K. Hinsen and B. Roux, *J. Comput. Chem.*, **18**, 368 (1997).
53. B. R. Brooks, R. E. Bruccoleri, B. D. Olafson, S. Swaminathan, D. J. States, and M. Karplus, *J. Comput. Chem.*, **4**, 187 (1983).
54. M. J. Frisch, M. Head-Gordon, G. W. Trucks, J. B. Foresman, H. B. Schlegel, K. Raghavachari, M. Robb, J. S. Binkley, C. Gonzalez, D. J. Defrees, D. J. Fox, R. A. Whiteside, R. Seeger, C. F. Melius, J. Baker, R. L. Martin, L. R. Kahn, J. J. P. Stewart, S. Topiol, and J. A. Pople, *GAUSSIAN*, Gaussian, Inc., Pittsburgh, PA 1990.
55. M. D. Feit, J. A. Fleck, Jr., and A. Steiger, *J. Comput. Phys.*, **47**, 412 (1982).
56. W. H. Press, S. A. Teukolsky, W. T. Vetterling, and B. P. Flannery, *Numerical Recipe in C*, Cambridge University Press, Cambridge, UK, 1992.
57. R. Kosloff and H. Tal-Ezer, *Chem. Phys. Lett.*, **127**, 223 (1986).
58. M. P. Allen and D. J. Tildesley, *Computer Simulations of Liquids*, Clarendon Press, Oxford, 1987.
59. F. Webster, P. J. Rossky, and R. A. Friesner, *Comput. Phys. Commun.*, **63**, 494 (1991).
60. N. Makri and W. H. Miller, *J. Chem. Phys.*, **87**, 5781 (1987).
61. H. D. Meyer, U. Manthe, and L. S. Cederbaum, *Chem. Phys. Lett.*, **165**, 73 (1990).
62. U. Manthe, H. D. Meyer, and L. S. Cederbaum, *Chem. Phys. Lett.*, **97**, 9062 (1992).